

## Extraordinary low systematic frequency shifts in bi-colour thulium optical clock

A. Golovizin,<sup>1a)</sup> and D. Tregubov,<sup>1</sup> E. Fedorova,<sup>1</sup> D. Mishin,<sup>1</sup> D. Provorchenko,<sup>1</sup>  
K. Khabarova,<sup>1,2</sup> V. Sorokin,<sup>1</sup> N. Kolachevsky<sup>1,2</sup>

<sup>1</sup> *P.N. Lebedev Physical Institute, Leninsky prospekt 53, 119991 Moscow, Russia*

<sup>2</sup> *Russian Quantum Center, Bolshoy Bulvar 30, bld. 1, Skolkovo IC, 121205 Moscow, Russia*

(Dated: 16 February 2021)

Optical atomic clocks have already overcome the eighteenth decimal digit of instability and uncertainty demonstrating incredible control over external perturbations of the clock transition frequency<sup>1-6</sup>. At the same time there is an increasing demand for atomic and ionic transitions with minimal sensitivity to external fields, with practical operational wavelengths and robust readout protocols<sup>7-10</sup>. One of the goals is to simplify clock's operation maintaining its relative uncertainty at low  $10^{-18}$  level. It is especially important for transportable and envisioned space-based optical clocks<sup>11,12</sup>. We proved earlier<sup>13,14</sup> that the  $1.14 \mu\text{m}$  inner-shell magnetic dipole transition in neutral thulium possesses very low blackbody radiation shift compared to other neutrals. Here we demonstrate operation of a bi-colour thulium optical clock with extraordinary low sensitivity to the Zeeman shift due to a simultaneous interrogation of two clock transitions and data processing. Our experiment shows suppression of the quadratic Zeeman shift by at least three orders of magnitude. The effect of tensor lattice Stark shift can be also reduced to below  $10^{-18}$  in fractional frequency units. All these features make thulium optical clock almost free from hard-to-control systematic shifts. Together with convenient cooling and trapping laser wavelengths, it provides great perspectives for thulium lattice clock as a high-performance transportable system.

---

<sup>a)</sup>Electronic mail: artem.golovizin@gmail.com

Excellent applicability of atoms as frequency references owes to high-quality factor of certain atomic transitions and possibility to isolate atoms from the environment. The first atomic microwave frequency reference<sup>15</sup> was demonstrated in 1955, and in 1967 the SI second was redefined<sup>16</sup> (9.2 GHz hyperfine transition in Cs). Later, advances in laser technology, manipulation of atoms and ions and optical frequency measurements paved a way to high-Q optical frequency references<sup>17–19</sup>. Modern optical clocks operating at  $10^{-18}$  level of relative instability and uncertainty<sup>6,20–22</sup> stimulate discussion about inevitable redefinition of the SI second<sup>23,24</sup>, which is also motivated by comparisons of different types of optical clocks at  $10^{-17}$  level<sup>20,21,25,26</sup>. Such performance allows to accurately test some fundamental physical theories: general relativity<sup>27,28</sup>, Lorentz invariance<sup>29,30</sup>, drifts of fundamental constants<sup>31,32</sup>, search for the dark matter particles<sup>33</sup> and dark matter clusters<sup>34</sup>.

High-performance transportable optical clocks are considered as an essential part of a worldwide optical clocks network<sup>28,35</sup>. Together with stabilized optical fibre links<sup>21,36</sup>, transportable systems are requested for long-distant time and frequency comparisons and chronometric levelling<sup>27,28</sup>. The most advanced systems are based on single ions in Paul traps and ensembles of neutral atoms in optical lattices. Single-ion systems are typically less sensitive to the environment and allow simpler setups, while clocks based on ensembles of neutral atoms (typically up to  $10^5$ ) demonstrate a better stability. Largest systematic shifts in lattice clocks come from the lattice and interrogation light fields, blackbody radiation (BBR), and an external magnetic field (the Zeeman shift)<sup>27,28,37</sup>. In this paper we demonstrate that all above mentioned shifts can be reduced to  $10^{-18}$  level or lower in thulium bi-colour lattice optical clock.

The advantageous metrological properties of the  $1.14\ \mu\text{m}$  inner shell clock transition in  $^{169}\text{Tm}$  are associated with similarity of the clock levels and their wave functions. The clock levels are the fine-structure components of the same ground state electronic level separated by the optical interval of  $1.14\ \mu\text{m}$ . The transition is associated with a spin flip in the  $4f$ -electron shell, which is strongly shielded by the outer closed  $5s^2$  and  $6s^2$  shells (Fig. 1a). Both factors make the transition frequency highly insensitive to the  $dc$  external electric field and collisions, which was first experimentally observed already in 1983<sup>38</sup>. We showed previously<sup>13,14</sup> that the  $1.14\ \mu\text{m}$  ( $\nu_0 = 2.6 \times 10^{14}$  Hz) transition possesses very small susceptibility to a  $dc$  external electric field which provides very low sensitivity to black body radiation (BBR). At the room temperature the BBR frequency shift corresponds to only

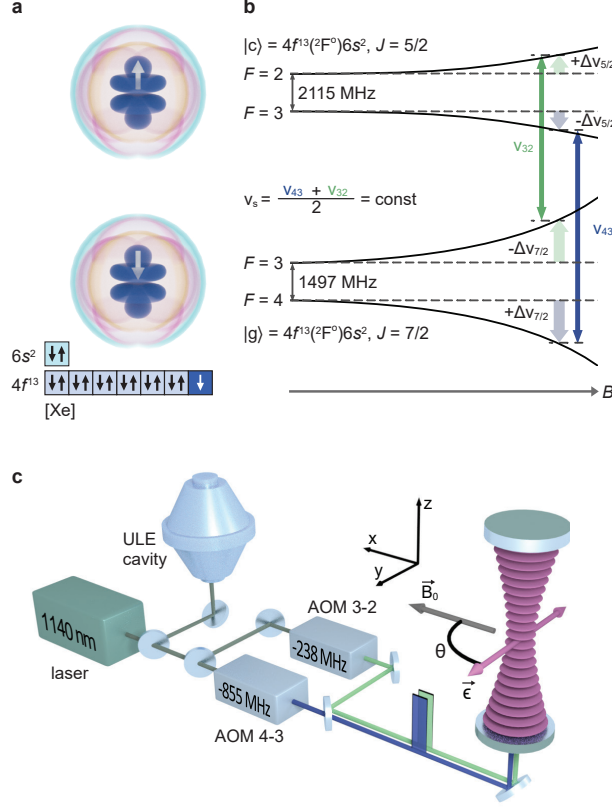


FIG. 1. Bi-color interrogation scheme in Tm clock using the hyperfine components of the clock levels. a) Visual representation of electronic structure of the ground and clock levels. Unpaired 4f-electron is located inside of the closed 6s shell. White arrow represents spin orientation of the electron. b) magnetic doublets of the ground- and excited-states clock levels. Two simultaneously interrogated transition frequencies are denoted as  $\nu_{43}$  and  $\nu_{32}$ . c) sketch of the experimental setup. The 1.14  $\mu\text{m}$  laser is stabilized to ULE cavity. Two acousto-optic modulators (AOMs) form pulse sequences for the simultaneous "4-3" and "3-2" clock transitions interrogation of atoms trapped in the vertically-oriented optical lattice at 1064 nm.

$2.3(1.1) \times 10^{-18}$  in fractional units which is thousands of times smaller than, e.g. in strontium lattice clock. We also observed close-to-zero differential polarizability of the clock levels of 0.00 (0.01) a.u. at 1064 nm, which indicates the proximity of the magic wavelength in a very practical spectral region where powerful and low-noise fiber lasers are available. This magic wavelength has a number of useful features. The polarizability slope of  $10^{-3}$  a.u./nm at 1064 nm is three orders of magnitude smaller than for  $^{87}\text{Sr}$  at the magic wavelength 813 nm<sup>39</sup>. This significantly softens the requirements to the lattice laser frequency stabi-

lization (GHz instead of MHz range). Large detuning from any transition frequency in Tm and the absence of the close-to-resonant terms in hypopolarizability<sup>13</sup> should also result in much smaller multipolar polarizability  $\Delta\alpha_{M1+E2}$  and hyperpolarizability  $\beta$  compared to <sup>87</sup>Sr. Note, that at the same time in Sr optical clocks the lattice shifts can be suppressed to the low  $10^{-18}$  level<sup>39,40</sup>.

Yet the advantages of the  $4f$ -shell clock transition come with a price: asymmetric structure of the electron wave-function and the strong magnetic dipole-dipole interaction. The contribution from the dipole-dipole interaction can be readily cancelled out by use of transition between zero projections of total atomic momentum  $m_F = 0 \rightarrow m_F = 0$ . The asymmetric wave function results in a non-zero differential tensor polarizability which is numerically small (0.2 a.u. at 1064 nm), but significant at the requested level of uncertainty. Still, the key systematic contribution to the frequency shift of the  $4f$ -shell clock transition is the second order Zeeman shift of 257 Hz/G<sup>2</sup> which is large compared to other atomic species used in optical clocks. Exactly these two effects — the Zeeman effect and the tensor polarizability — in our case account for the main undesired systematic contributions. Handling these two shifts simultaneously requires unconventional approach because of their opposite behaviour with respect to the bias magnetic field  $B_0$ . Decreasing of the bias magnetic field reduces the quadratic Zeeman shift and corresponding uncertainty, while uncertainty of the tensor Stark shift generally increases.

Here we propose and experimentally implement a method for complete cancellation of the Zeeman shift and for the tight control over the tensor polarizability shift at lower than 1 mHz level which corresponds to  $3.8 \times 10^{-18}$  in relative frequency units. This approach provides extremely low, compared to other widespread optical clocks, net systematic frequency shift and corresponding uncertainty in Tm system at  $10^{-18}$  level. The idea is to use simultaneous bi-colour interrogation scheme of two ground-state hyperfine sublevels  $F = 4$  and  $F = 3$  which allows to use the instantaneous synthetic frequency

$$\nu_s = \frac{\nu_{43} + \nu_{32}}{2} \quad (1)$$

as depicted in Fig. 1b. Here  $\nu_{43}$  and  $\nu_{32}$  are the frequencies of the  $|g, F = 4, m_F = 0\rangle \rightarrow |c, F = 3, m_F = 0\rangle$  (short notation "4-3") and  $|g, F = 3, m_F = 0\rangle \rightarrow |c, F = 2, m_F = 0\rangle$  ("3-2") transitions, respectively. Here  $|g\rangle$  stands for the  $|4f^{13}(^2F^o)6s^2, J = 7/2\rangle$  ground level and  $|c\rangle$  stands for the  $|4f^{13}(^2F^o)6s^2, J = 5/2\rangle$  clock level. It turns out that the synthetic

frequency  $\nu_s$  is completely insensitive to the magnetic field because of equal but opposite Zeeman shifts of "4-3" and "3-2" clock transitions (see Supplementary for details).

Synthetic frequency is used on a regular basis in various optical clocks when different magnetic sublevels are interrogated successively<sup>41</sup>. However proposed approach possesses an important advantage: in our configuration we simultaneously probe two hyperfine clock transitions, such that the impact of fluctuating external magnetic field on two frequencies becomes completely identical. This fact results in a full cancellation of the Zeeman shift without any assumptions about magnetic field behaviour between consecutive measurements. To successfully implement this approach one should (i) simultaneously prepare an atomic ensemble in two initial states, and (ii) independently and simultaneously interrogate and readout two hyperfine clock transitions every measurement cycle.

Simultaneous single-frequency optical pumping to  $|F = 3, 4, m_F = 0\rangle$  central magnetic sublevels was demonstrated in our previous work<sup>42</sup>. In turn, relatively small separation of the clock transition frequencies of  $\Delta\nu = \nu_{32} - \nu_{43} \approx 617$  MHz simplifies simultaneous interrogation and readout using acousto-optical modulators (AOMs). At the same time, the *ac* Stark shift induced by the bi-colour probe field is only  $0.06 \mu\text{Hz}$  in our experimental conditions because of the low probe field intensity. The mutual influence of interrogation and readout fields in the bi-colour scheme is discussed in Supplementary. It is also worth mentioning that polarizabilities of  $m_F = 0$  sublevels in the hyperfine doublets are identically equal such that the condition for the magic wavelength fulfils simultaneously for both clock transitions.

### **Zeroing the Zeeman shift in the bi-colour scheme**

We prepare approximately  $10^5$  atoms in the  $|g, F = 4, m_F = 0\rangle$  state and  $10^4$  atoms in the  $|g, F = 3, m_F = 0\rangle$  state using simultaneous optical pumping<sup>42</sup> with a following lattice depth ramp to sift out hot atoms from the trap. Two clock transitions are simultaneously excited by 80 ms-long clock laser  $\pi$ -pulses with the frequencies  $\nu_{43}$  and  $\nu_{32}$  separated by approximately 617 MHz. Using the readout procedure described in Supplementary, we simultaneously measure the excitation probability for each of the transition for certain probe field detunings. We prove that our experimental procedure allows to independently deduce two excitation efficiencies. The system operates in the classical optical clock regime, when the laser frequency is alternatively switched between the left and the right slope of the clock transition. In our case the spectral linewidth of both clock transitions is  $\delta\nu = 10$  Hz. Using

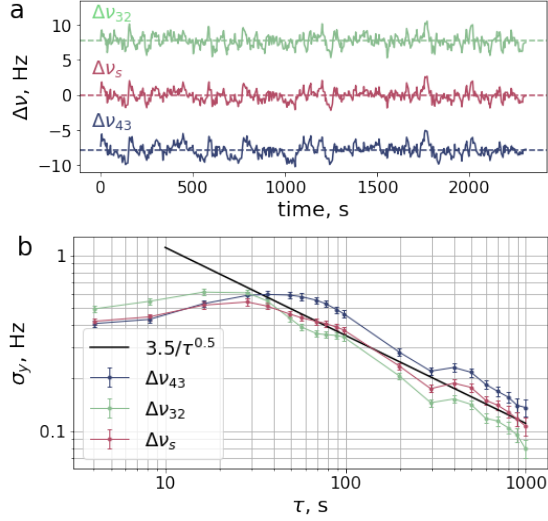


FIG. 2. a) Measurement of clock transitions frequency shifts  $\Delta\nu_{43} = \nu_{43}(B^m) - \nu_{43}(B^r)$  (blue) and  $\Delta\nu_{32} = \nu_{32}(B^m) - \nu_{32}(B^r)$  (green) for two alternatively changing values of the bias magnetic field  $B_0^r = 218$  mG and  $B_0^m = 132$  mG. Common features in  $\Delta\nu_{43}$  and  $\Delta\nu_{32}$  data sets come from clock laser frequency fluctuations. The synthetic frequency shift  $\Delta\nu_s = (\Delta\nu_{43} + \Delta\nu_{32})/2$  is plotted in red with the mean value of  $-0.08(6)$  Hz (dashed line). b) The Allan variance plotted for each of the data sets. The solid black line indicates  $\sim 1/\sqrt{\tau}$  dependency.

this method we deduce two independent error signals and two clock transition frequencies  $\nu_{43}$  and  $\nu_{32}$ . As a stable frequency reference we use  $1.14 \mu\text{m}$  clock cavity with the linear drift correction<sup>43</sup>. The impact of an external parameter (e.g. the bias magnetic field  $B_0$ ) on the transition frequency can be studied by differential measurement when the parameter is changed alternatively between two values for odd and even measurement cycles. The multi-channel digital lock tracks corresponding transition frequencies. Calibrating measurements are periodically performed in order to monitor and tune auxiliary parameters (see Supplementary).

In order to experimentally verify cancellation of the Zeeman shift for the synthetic frequency  $\nu_s$ , we change the bias magnetic field between two largely different values: the “reference” field  $B_0^r = 218$  mG and the “main” field  $B_0^m = 132$  mG. The digital locks track corresponding frequency shifts with the help of the AOMs (see Fig.1c). We deduce differen-

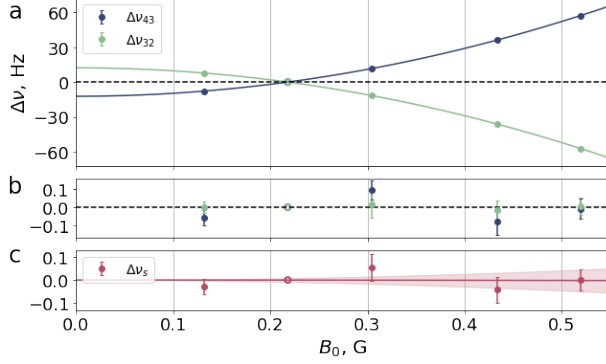


FIG. 3. Zeeman frequency shifts. a) Frequency shifts  $\Delta\nu_{43}$  and  $\Delta\nu_{32}$  as a function of the “main” bias magnetic fields  $B_0^m$  at the fixed value of the “reference” field of  $B_0^r = 218 \text{ mG}$ . Solid lines are the parabolic fits to the data. b) The fit residuals. The synthetic frequency shift  $\Delta\nu_s$  is shown in c). The shaded area indicates  $1\sigma = 0.175 \text{ Hz/G}^2$  uncertainty of the quadratic Zeeman coefficient.

tial frequency shifts of two clock transitions

$$\begin{aligned}\Delta\nu_{43} &= \nu_{43}(B^m) - \nu_{43}(B^r), \\ \Delta\nu_{32} &= \nu_{32}(B^m) - \nu_{32}(B^r)\end{aligned}\tag{2}$$

and the corresponding synthetic frequency shift

$$\Delta\nu_s = (\Delta\nu_{43} + \Delta\nu_{32})/2.\tag{3}$$

The frequency differences  $\Delta\nu_{43}$ ,  $\Delta\nu_{32}$ , and  $\Delta\nu_s$  measured for 2300 s are shown in Fig. 2a. The mean value for  $\Delta\nu_{43}$  equals to  $-7.88(9) \text{ Hz}$ , while for  $\Delta\nu_{32}$  it equals to  $+7.72(7) \text{ Hz}$ , where the number in parentheses indicates one standard deviation. For the synthetic frequency the effect averages out to  $-0.08(6) \text{ Hz}$ . Figure 2b shows the Allan variance for the corresponding data sets. For longer averaging times we see the  $3.5 \times \tau^{-1/2} \text{ Hz}$  behaviour for  $\Delta\nu_s$  which corresponds to  $1.4 \times 10^{-14} \tau^{-1/2}$  (here  $\tau$  is taken in seconds) in relative units. For short averaging times of 1 s the Allan variance approaches instability of the clock laser of  $2 \times 10^{-15}$  which was characterized earlier<sup>44</sup>. Fluctuations of interrogation laser and the performance of digital locks are discussed in Supplementary.

Similar measurements were done for different values of the “main” bias magnetic field  $B_0^m$  in the range of 130 – 520 mG at the fixed value  $B_0^r = 218 \text{ mG}$ . Corresponding data for  $\Delta\nu_{43}$ ,  $\Delta\nu_{32}$ , as well as for the synthetic frequency shift  $\Delta\nu_s$ , are shown in Fig. 3a. The frequency dependencies  $\Delta\nu_{43}(B_0^m)$  and  $\Delta\nu_{32}(B_0^m)$  are fitted by the parabolic function

in the form  $\beta(B_0^m - B_0^r)$ , where  $\beta$  is the quadratic Zeeman coefficient. We get  $\beta_{43} = +257.47(22)(75)$  Hz/G<sup>2</sup> and  $\beta_{32} = -257.42(18)(75)$  Hz/G<sup>2</sup>. The value in the first parentheses represents  $1\sigma$  statistical error of the fit. The value in the second parentheses corresponds to  $1\sigma$  uncertainty due to the measurement error of the bias magnetic field (see Supplementary for the details). The absolute values of  $\beta_{43}$  and  $\beta_{32}$  are equal within the combined uncertainty. The averaged value  $\beta = 257.44(14)(75)$  Hz/G<sup>2</sup> agrees with the calculated value<sup>14</sup> of  $\beta^{\text{th}} = 257.2$  Hz/G<sup>2</sup>.

The synthetic frequency shift depicted in Fig. 3c is also fitted by the parabolic function which gives  $\beta_s = -0.008(185)$  Hz/G<sup>2</sup>. It is compatible with zero within the measurement uncertainty and corresponds to at least 1000-fold reduction in sensitivity to the Zeeman shift compared to an individual clock transition.

### Tensor Stark shift from the optical lattice field

The Zeeman shift cancellation opens a way to improve control on the tensor Stark shift. The tensor part of the clock transition frequency shift from the optical lattice is given by

$$\Delta\nu^t = \tilde{\alpha}^t \times (3 \cos^2 \theta - 1) \times (U/E_r), \quad (4)$$

where  $\theta$  is the angle between the bias magnetic field  $\vec{B}_0$  and the lattice polarization vector  $\vec{\epsilon}$ , as shown in Fig. 1c. Here  $U$  is the lattice depth,  $E_r = \hbar^2 k^2 / (2m) = h \times 1043$  Hz is the lattice photon recoil energy. The coefficient  $\tilde{\alpha}^t$  is associated with the differential tensor polarizability of  $-0.20(4)$  a.u. of the  $1.14 \mu\text{m}$  transition in Tm at  $1064 \text{ nm}$ <sup>14</sup> and is evaluated to be  $0.7$  Hz (see Supplementary). In our experiment, a 1D optical lattice at  $1064 \text{ nm}$  is aligned vertically along the  $z$  axis, its polarisation  $\vec{\epsilon}$  is parallel to the  $y$  axis and  $\vec{B}_0$  is parallel to the  $x$  axis, such that the angle  $\theta$  is close to  $\pi/2$  (see Fig. 1c). Since  $\Delta\nu^t$  has maximum for  $\theta_0 = \pi/2$ , its sensitivity to small fluctuation  $\delta\theta$  around  $\theta_0$  can be approximated by

$$\delta^t = \Delta\nu^t(\pi/2 + \delta\theta) - \Delta\nu^t(\pi/2) = 3\tilde{\alpha}^t(U/E_r) \times \delta\theta^2 \quad (5)$$

assuming the constant value of  $U$ . For the typical trap depth of  $U = 100 E_r$ , accurate control of  $\delta^t$  below  $1$  mHz requires  $|\delta\theta| \lesssim 10^{-3}$ . In our configuration  $\delta\theta = B_y/B_0$  assuming that the direction of lattice polarisation is much more stable than the direction of the external magnetic field. To reduce  $\delta^t$  it is necessary to increase the bias magnetic field  $B_0$ .

Using the bi-colour scheme we actively stabilize  $\theta$  to  $\pi/2$  using the following method. During a typical measurement run, we perform the perpendicular magnetic field calibration



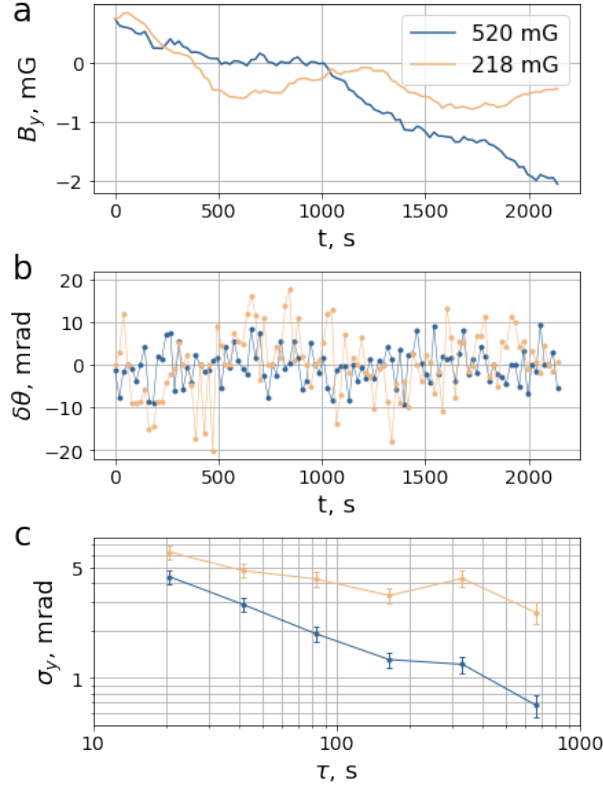


FIG. 4. Stabilization of the bias magnetic field direction. a) Compensation field  $B_y$  as a function of time for one measurement run. The orange line corresponds to the data points with the “reference” field  $B_0^r = 218$  mG, the blue line — to the points with “main” field  $B_0^m = 520$  mG. b) Evaluated  $\delta\theta$  over the measurement run. c) The Allan variance for  $\delta\theta$  data sets from b).

every 5th cycle. Clock transition frequency shifts  $\delta_{\pm}^t$  are measured for two opposite signs of the deliberately added/subtracted increment  $\Delta\theta$  which gives  $\theta = \pi/2 + \delta\theta \pm \Delta\theta$ . The increment  $\Delta\theta \approx 0.1$  is added by changing the perpendicular magnetic field  $B_y$ . This method significantly increases sensitivity of the frequency shift from  $\sim \delta\theta^2$  dependency to  $\sim \delta\theta\Delta\theta$ . The misalignment  $\delta\theta$  is deduced from the frequency mismatch  $\delta_+^t - \delta_-^t$  (see Supplementary for details). Note, that fluctuations of the magnetic field along  $z$  axis do not influence angle  $\theta$ .

Figure 4a shows traces of perpendicular magnetic field  $B_y$  produced by the compensation coils. For the given run we apply  $B_0^r = 218$  mG and  $B_0^m = 520$  mG. Depending on the value of the bias field (“reference” or “main”), different values of the compensation field are applied which are indicated as orange and blue lines, correspondingly. Plots on Fig. 4b show the

misalignment angle  $\delta\theta$  which is deduced from corresponding magnetic field measurements (see Supplementary). Corresponding Allan variance for  $\delta\theta$  data sets is shown in Fig. 4c. For larger bias magnetic field  $B_0^m = 520$  mG, fluctuations of  $\delta\theta$  are smaller. In this case the uncertainty of  $\delta\theta = 1$  mrad is achieved after 500 seconds integration. For  $B_0^r = 218$  mG the averaging goes slower due to larger shot-to-shot fluctuations. Using these results one can evaluate contribution of the tensor Stark shift from the optical lattice (the lattice depth  $U = 300 E_r$ ) using Eq. 5. We get corresponding contribution to the fractional frequency uncertainty of  $\delta^t/\nu_0 < 10^{-17}$  for  $B_0^r = 218$  mG and  $\delta^t/\nu_0 < 10^{-18}$  for  $B_0^m = 520$  mG after 500 seconds of integration. Note, that the increase of the bias magnetic field does not lead to additional Zeeman shift-associated uncertainty because of the bi-colour operation scheme.

### Discussion

In this work we report on extraordinary low overall systematic frequency shifts in Tm optical clock operating at  $1.14 \mu\text{m}$  inner-shell magnetic dipole transition. In the bi-colour operation scheme we online measure the synthetic frequency  $\nu_s = (\nu_{43} + \nu_{32})/2$  based on the simultaneous interrogation of two ground-state hyperfine components. We have proven that the synthetic frequency allows to cancel out contribution of the Zeeman shift without any assumptions about magnetic field fluctuations. The experiments show that the Zeeman shift of the synthetic frequency is consistent with zero within currently achievable statistical uncertainty, confirming the suppression of the quadratic Zeeman shift at least for 1000 times. Using this technique we have experimentally demonstrated that contribution of the tensor Stark shift induced by the optical lattice can be also reduced to  $10^{-18}$  level by accurate online tuning of the magnetic field direction. Together with results from ref.<sup>14</sup> demonstrating very low sensitivity of Tm clock transition to the BBR shift ( $2.3 \times 10^{-18}$  at the room temperature), the suggested bi-colour Tm optical clock becomes almost free from systematic frequency shifts at  $10^{-18}$  level.

The operational magic wavelength around 1064 nm promises further advantages compared to many other optical lattice clocks. First, powerful and low-noise fiber lasers are available in this spectral region. Second, the sensitivity to the lattice wavelength is very low (1000 times smaller compared to Sr optical clock), which results in smaller lattice shifts from higher-order terms. Summing up, bi-colour Tm optical clock operating at the  $1.14 \mu\text{m}$  inner-shell magnetic dipole transition demonstrates its functional capacity for the next generation of transportable systems with very moderate requirements to environmental conditions,

temperature and magnetic field fluctuations.

## I. ACKNOWLEDGMENTS

Authors acknowledge support from RSF grant #19-12-00137. Authors are grateful to Denis Sukachev for careful reading and valuable discussion of the manuscript.

## REFERENCES

- <sup>1</sup>N. Huntemann, C. Sanner, B. Lipphardt, Chr. Tamm, and E. Peik. Single-Ion Atomic Clock with  $3 \times 10^{-18}$  Systematic Uncertainty. *Physical Review Letters*, 116(6):063001, 2016.
- <sup>2</sup>W. F. McGrew, X. Zhang, R. J. Fasano, S. A. Schäffer, K. Beloy, D. Nicolodi, R. C. Brown, N. Hinkley, G. Milani, M. Schioppo, T. H. Yoon, and A. D. Ludlow. Atomic clock performance enabling geodesy below the centimetre level. *Nature*, 564(7734):87–90, 2018.
- <sup>3</sup>S M Brewer, J Chen, A M Hankin, E R Clements, C W Chou, D J Wineland, D B Hume, and D R Leibbrandt. An  $^{27}\text{Al}$  + quantum-logic clock with systematic uncertainty below  $10^{-18}$ . *Phys. Rev. Lett.*, 123:033201, 2019.
- <sup>4</sup>Tobias Bothwell, Dhruv Kedar, Eric Oelker, John M Robinson, Sarah L Bromley, Weston L Tew, Jun Ye, and Colin J Kennedy. JILA SrI optical lattice clock with uncertainty of  $2.0 \times 10^{-18}$ . *Metrologia*, 56:065004 (16pp), 2019.
- <sup>5</sup>M. Schioppo, R.C. Brown, W.F. McGrew, N. Hinkley, R.J. Fasano, K. Beloy, T.H. Yoon, G. Milani, D. Nicolodi, J.A. Sherman, N.B. Phillips, C.W. Oates, and A.D. Ludlow. Ultra-stable optical clock with two cold-atom ensembles. *Nature*, 11:48–82, 2017.
- <sup>6</sup>E. Oelker, R. B. Hutson, C. J. Kennedy, L. Sonderhouse, T. Bothwell, A. Goban, D. Kedar, C. Sanner, J. M. Robinson, G. E. Marti, D. G. Matei, T. Legero, M. Giunta, R. Holzwarth, F. Riehle, U. Sterr, and J. Ye. Demonstration of  $4.8 \times 10^{-17}$  stability at 1 s for two independent optical clocks. *Nature Photonics*, 13(10):714–719, 2019.
- <sup>7</sup>Corey J Campbell, Alexander G Radnaev, A Kuzmich, Vladimir A Dzuba, Victor V Flambaum, and Andrei Derevianko. Single-ion nuclear clock for metrology at the 19th decimal place. *Physical review letters*, 108(12):120802, 2012.
- <sup>8</sup>Nozomi Ohtsubo, Ying Li, Kensuke Matsubara, Nils Nemitz, Hidekazu Hachisu, Tetsuya Ido, and Kazuhiro Hayasaka. Optical clock based on a sympathetically-cooled indium ion.

- Hyperfine Interactions*, 240(1):1–8, 2019.
- <sup>9</sup>K. J. Arnold, R. Kaewuam, A. Roy, T. R. Tan, and M. D. Barrett. Blackbody radiation shift assessment for a lutetium ion clock. *Nature Communications*, 9(1):1–6, 2018.
- <sup>10</sup>P Micke, T Leopold, SA King, E Benkler, LJ Spieß, Lisa Schmoeger, M Schwarz, JR Crespo López-Urrutia, and PO Schmidt. Coherent laser spectroscopy of highly charged ions using quantum logic. *Nature*, 578(7793):60–65, 2020.
- <sup>11</sup>Pacôme Delva, Aurélien Hees, and Peter Wolf. Clocks in Space for Tests of Fundamental Physics. *Space Science Reviews*, 212(3-4):1385–1421, 11 2017.
- <sup>12</sup>S. Schiller, P. Lemonde, G. M. Tino, U. Sterr, Ch. Lisdat, A. Görlitz, N. Poli, A. Nevsky, and C. Salomon. The space optical clocks project. *International Conference on Space Optics — ICSO 2010*, 10565:47, 11 2017.
- <sup>13</sup>D. Sukachev, S. Fedorov, I. Tolstikhina, E. Kalganova, G. Vishnyakova, K. Khabarova, D. Tregubov, A. Golovizin, V. Sorokin, and N. Kolachevsky. Inner-shell magnetic dipole transition in Tm atom as a candidate for optical lattice clocks. *Phys. Rev. A.*, 94(2), 2016.
- <sup>14</sup>A Golovizin, E Fedorova, D Tregubov, D Sukachev, K Khabarova, V Sorokin, and N Kolachevsky. Inner-shell clock transition in atomic thulium with a small blackbody radiation shift. *Nature Communications*, 10:1–8, 2019.
- <sup>15</sup>Louis Essen and Jack VL Parry. An atomic standard of frequency and time interval: a caesium resonator. *Nature*, 176(4476):280–282, 1955.
- <sup>16</sup>J Terrien. News from the international bureau of weights and measures. *Metrologia*, 4(1):41, 1968.
- <sup>17</sup>Nicola Poli, CW Oates, Patrick Gill, and GM Tino. Optical atomic clocks. *La rivista del Nuovo Cimento*, 36, 6 2013.
- <sup>18</sup>A.D. Ludlow, M.M. Boyd, J. Ye, E. Peik, and P.O. Schmidt. Optical Atomic Clocks. *Reviews of Modern Physics*, 87(2):637, 2015.
- <sup>19</sup>Th Udem, R. Holzwarth, and T. W. Hänsch. Optical frequency metrology. *Nature*, 416(6877):233–237, 2002.
- <sup>20</sup>N Ohmae, F Bregolin, N Nemitz, and H Katori. Direct measurement of the frequency ratio for Hg and Yb optical lattice clocks and closure of the Hg / Yb / Sr loop. *Optics Express*, 28(10):15112–15121, 2020.
- <sup>21</sup>Boulder Atomic Clock Optical Network, Collaboration, :, Kyle Beloy, Martha I Bodine, Tobias Bothwell, Samuel M Brewer, Sarah L. Bromley, Jwo-sy Chen, Jean-Daniel Deschênes,

- Scott A Diddams, Robert J Fasano, Tara M Fortier, Youssef S Hassan, David B Hume, Dhruv Kedar, Colin J Kennedy, Isaac Khader, Amanda Koepke, David R. Leibbrandt, Holly Leopardi, Andrew D Ludlow, William F. McGrew, William R Milner, Nathan R Newbury, Daniele Nicolodi, Eric Oelker, Thomas E Parker, John M Robinson, Stefania Romisch, Stefan A. Schäffer, Jeffrey A Sherman, Laura C Sinclair, Lindsay Sonderhouse, William C Swann, Jian Yao, Jun Ye, and Xiaogang Zhang. Frequency Ratio Measurements with 18-digit Accuracy Using a Network of Optical Clocks. *arXiv*, 5 2020.
- <sup>22</sup>William R Milner, John M Robinson, Colin J Kennedy, Tobias Bothwell, Dhruv Kedar, Dan G Matei, Thomas Legero, Uwe Sterr, Fritz Riehle, Holly Leopardi, et al. Demonstration of a timescale based on a stable optical carrier. *Physical review letters*, 123(17):173201, 2019.
- <sup>23</sup>Fritz Riehle, Patrick Gill, Felicitas Arias, and Lennart Robertsson. The CIPM list of recommended frequency standard values: Guidelines and procedures. *Metrologia*, 55(2):188–200, 2018.
- <sup>24</sup>Jérôme Lodewyck. On a definition of the si second with a set of optical clock transitions. *Metrologia*, 56(5):055009, 2019.
- <sup>25</sup>N. Nemitz, T. Ohkubo, M. Takamoto, I. Ushijima, M. Das, N. Ohmae, and H. Katori. Frequency ratio of Yb and Sr clocks with  $5 \times 10^{-17}$  uncertainty at 150 seconds averaging time. *Nature Photonics*, 10(4):258–261, 2016.
- <sup>26</sup>S. Dörscher, N. Huntemann, R. Schwarz, R. Lange, E. Benkler, B. Lipphardt, U. Sterr, E. Peik, and C. Lisdat. Optical frequency ratio of a  $171\text{Yb}^+$  single-ion clock and a  $87\text{Sr}$  lattice clock. *Metrologia*, 58(1):8, 2 2021.
- <sup>27</sup>Masao Takamoto, Ichiro Ushijima, Noriaki Ohmae, Toshihiro Yahagi, Kensuke Kokado, Hisaaki Shinkai, and Hidetoshi Katori. Test of general relativity by a pair of transportable optical lattice clocks. *Nature Photonics*, 14(7):411–415, 2020.
- <sup>28</sup>Jacopo Grotti, Silvio Koller, Stefan Vogt, Sebastian Häfner, Uwe Sterr, Christian Lisdat, Heiner Denker, Christian Voigt, Ludger Timmen, Antoine Rolland, Fred N. Baynes, Helen S. Margolis, Michel Zampaolo, Pierre Thoumany, Marco Pizzocaro, Benjamin Rauf, Filippo Bregolin, Anna Tampellini, Piero Barbieri, Massimo Zucco, Giovanni A. Costanzo, Cecilia Clivati, Filippo Levi, and Davide Calonico. Geodesy and metrology with a transportable optical clock. *Nature Physics*, 14(5):437–441, 2018.

- <sup>29</sup>Christian Sanner, Nils Huntemann, Richard Lange, Christian Tamm, Ekkehard Peik, Marianna S. Safronova, and Sergey G. Porsev. Optical clock comparison for Lorentz symmetry testing. *Nature*, 567(7747):204–208, 3 2019.
- <sup>30</sup>R. Lange, N. Huntemann, J. M. Rahm, C. Sanner, H. Shao, B. Lipphardt, Chr. Tamm, S. Weyers, and E. Peik. Improved Limits for Violations of Local Position Invariance from Atomic Clock Comparisons. *Physical Review Letters*, 126(1):011102, 1 2021.
- <sup>31</sup>N. Huntemann, B. Lipphardt, Chr Tamm, V. Gerginov, S. Weyers, and E. Peik. Improved limit on a temporal variation of  $m_p/m_e$  from comparisons of Yb+ and Cs atomic clocks. *Physical Review Letters*, 113(21), 2014.
- <sup>32</sup>R. M. Godun, P. B.R. Nisbet-Jones, J. M. Jones, S. A. King, L. A.M. Johnson, H. S. Margolis, K. Szymaniec, S. N. Lea, K. Bongs, and P. Gill. Frequency ratio of two optical clock transitions in Yb+ 171 and constraints on the time variation of fundamental constants. *Physical Review Letters*, 113(21):1–5, 2014.
- <sup>33</sup>Colin J. Kennedy, Eric Oelker, John M. Robinson, Tobias Bothwell, Dhruv Kedar, William R. Milner, G. Edward Marti, Andrei Derevianko, and Jun Ye. Precision Metrology Meets Cosmology: Improved Constraints on Ultralight Dark Matter from Atom-Cavity Frequency Comparisons. *Physical Review Letters*, 125(20):201302, 11 2020.
- <sup>34</sup>B. M. Roberts, P. Delva, A. Al-Masoudi, A. Amy-Klein, C. Bærentsen, C. F.A. Baynham, E. Benkler, S. Bilicki, S. Bize, W. Bowden, J. Calvert, V. Cambier, E. Cantin, E. A. Curtis, S. Dörscher, M. Favier, F. Frank, P. Gill, R. M. Godun, G. Grosche, C. Guo, A. Hees, I. R. Hill, R. Hobson, N. Huntemann, J. Kronjäger, S. Koke, A. Kuhl, R. Lange, T. Legero, B. Lipphardt, C. Lisdat, J. Lodewyck, O. Lopez, H. S. Margolis, H. Álvarez-Martínez, F. Meynadier, F. Ozimek, E. Peik, P. E. Pottie, N. Quintin, C. Sanner, L. De Sarlo, M. Schioppo, R. Schwarz, A. Silva, U. Sterr, Chr Tamm, R. Le Targat, P. Tuckey, G. Vallet, T. Waterholter, D. Xu, and P. Wolf. Search for transient variations of the fine structure constant and dark matter using fiber-linked optical atomic clocks. *New Journal of Physics*, 22(9), 2020.
- <sup>35</sup>F. Riehle. Optical clock networks. *Nature Photonics*, 11(1):25–31, 2017.
- <sup>36</sup>C Lisdat, G Grosche, N Quintin, C Shi, S.M.F. Raupach, C Grebing, D. Nicolodi, F. Stefani, A. Al-Masoudi, S. Dörscher, S. Häfner, J.-L. Robyr, N. Chiodo, S. Bilicki, E. Bookjans, A. Koczwara, S. Koke, A. Kuhl, F. Wiotte, F. Meynadier, E. Camisard, M. Abgrall, M. Lours, T. Legero, H. Schnatz, U. Sterr, H. Denker, C. Chardonnet, Y. Le Coq,

- G. Santarelli, A. Amy-Klein, R. Le Targat, J. Lodewyck, O Lopez, and P.-E. Pottie. A clock network for geodesy and fundamental science. *Nature Communications*, 7(1):12443, 11 2016.
- <sup>37</sup>N. Poli, M. Schioppo, S. Vogt, St Falke, U. Sterr, Ch Lisdat, and G. M. Tino. A transportable strontium optical lattice clock. *Applied Physics B: Lasers and Optics*, 117(4):1107–1116, 2014.
- <sup>38</sup>EB Aleksandrov, VN Kotylev, KP Vasilevskii, and VN Kulyasov. 1.14- $\mu$ m thulium line unbroadened by collisions. *Optics and Spectroscopy*, 54(1):1, 1983.
- <sup>39</sup>Ichiro Ushijima, Masao Takamoto, and Hidetoshi Katori. Operational Magic Intensity for Sr Optical Lattice Clocks. *Physical Review Letters*, 121(26):198–201, 2018.
- <sup>40</sup>T. L. Nicholson, S. L. Campbell, R. B. Hutson, G. E. Marti, B. J. Bloom, R. L. McNally, W. Zhang, M. D. Barrett, M. S. Safronova, G. F. Strouse, W. L. Tew, and J. Ye. Systematic evaluation of an atomic clock at  $2 \times 10^{-18}$  total uncertainty. *Nature Communications*, 6, 2015.
- <sup>41</sup>J. E. Bernard, L. Marmet, and A. A. Madej. A laser frequency lock referenced to a single trapped ion. *Optics Communications*, 150(1-6):170–174, 1998.
- <sup>42</sup>E Fedorova, A Golovizin, D Tregubov, D Mishin, D Provorchenko, V Sorokin, K Khabarova, and N Kolachevsky. Simultaneous two initial clock states preparation for thulium optical clock. *arXiv preprint arXiv:2008.02050*, 2020.
- <sup>43</sup>A Golovizin, V Bushmakina, S Fedorov, E Fedorova, D Tregubov, D Sukachev, K Khabarova, V Sorokin, and N Kolachevsky. ULTRASTABLE LASER SYSTEM FOR SPECTROSCOPY OF THE 1 . 14  $\mu$  m INNER-SHELL CLOCK TRANSITION IN Tm AND ITS ABSOLUTE FREQUENCY MEASUREMENT. *Journal of Russian Laser Research*, 40(6):540–546, 2019.
- <sup>44</sup>I V Zalivako, I A Semerikov, A S Borisenko, M D Aksenov, P A Vishnyakov, P L Sidorov, N V Semenina, A A Golovizin, K Yu Khabarova, and N N Kolachevsky. Compact ultrastable laser system for spectroscopy of  $2 S 1/2 \rightarrow 2 D 3/2$  quadrupole transition in  $^{171}\text{Yb}^+$  ion. *Quantum Electronics*, 50(9):850–854, 2020.
- <sup>45</sup>D. Giggberger and S. Penselin. Ground-State Hyperfine Structure and Nuclear Magnetic Moment of Thulium-169. *Zeitschrift fuer Physik*, 255:244–255, 1967.

## THE SUPPLEMENTARY

**The Zeeman shift and the synthetic frequency.** The energy of an atomic level with the electronic momentum  $J$  and the nuclear spin  $I = 1/2$  in an external magnetic field  $B_0$  is given by<sup>13,45</sup>:

$$E_{J,F=J\pm 1/2,m_F} = -\frac{1}{4}hA_J + g_J\mu_B B_0 m_F \pm \frac{hA_J(2J+1)}{4} \sqrt{1 - \frac{4m_F}{2J+1}x + x^2}, \quad (6)$$

where  $A_J$  is the hyperfine splitting constant,  $x = \frac{2(g_J\mu_B - g_I\mu_N)B_0}{hA_J(2J+1)}$ ,  $g_J$  and  $g_I$  are the electronic and nuclear Landé g-factors,  $\mu_B$  and  $\mu_N$  are the Bohr and nuclear magnetons, correspondingly.

For the magnetic sublevel with zero projection  $m_F = 0$  and  $x \ll 1$  the level energy shift can be expressed as

$$\Delta E_{J,F=J\pm 1/2} = \pm \frac{(g_J\mu_B - g_I\mu_N)^2}{2hA_J(2J+1)} B_0^2 = \mp \beta_J B_0^2, \quad (7)$$

where  $\beta_J$  is the quadratic Zeeman shift coefficient for a given electronic level. The negative sign of  $A_J$  for the ground and the clock levels in thulium is taken into account. The coefficients  $\beta_{7/2} = 426 \text{ Hz/G}^2$  and  $\beta_{5/2} = 169 \text{ Hz/G}^2$  are relatively large due to small (1.5 GHz and 2.1 GHz, respectively) hyperfine splitting of the ground and clock levels. The frequencies of the  $|g, F = 4, m_F = 0\rangle \rightarrow |c, F = 3, m_F = 0\rangle$  and  $|g, F = 3, m_F = 0\rangle \rightarrow |c, F = 2, m_F = 0\rangle$  clock transitions as a function of  $B_0$  can be found as

$$\begin{aligned} h\Delta\nu_{43} &= \Delta E_{5/2,3} - \Delta E_{7/2,4} = -(\beta_{5/2} - \beta_{7/2})B_0^2, \\ h\Delta\nu_{32} &= \Delta E_{5/2,2} - \Delta E_{7/2,3} = (\beta_{5/2} - \beta_{7/2})B_0^2. \end{aligned} \quad (8)$$

Thus, for the synthetic frequency

$$\Delta\nu_s = \frac{\Delta\nu_{43} + \Delta\nu_{32}}{2} \quad (9)$$

the Zeeman shift completely cancels out. This result remains valid even without Taylor expansion of Eq. 6.



**The tensor polarizability coefficient.** Following Ref.<sup>14</sup>, an absolute value of the optical lattice trap depth can be expressed as

$$U = \left| -\alpha \frac{\mathcal{E}^2}{4} \right|, \quad (10)$$

where  $\mathcal{E}$  is the amplitude of the electric field and  $\alpha = 152$  a.u. (atomic units) is the ground level polarizability. The clock transition frequency shift from the tensor part of the polarizability is

$$h\Delta\nu^t = -\frac{3\cos^2\theta - 1}{2} \Delta\alpha^t \frac{\mathcal{E}^2}{4}. \quad (11)$$

Here  $\Delta\alpha^t = -0.2$  a.u.<sup>14</sup> for the lattice wavelength of 1064 nm. Inserting Eq. 10 to Eq. 11 and rearranging it, one gets

$$\Delta\nu^t = -(3\cos^2\theta - 1) \frac{U}{E_r} \times \frac{E_r}{2\alpha\hbar} \Delta\alpha^t. \quad (12)$$

Comparing this equation to Eq. 4 and using  $E_r = h \times 1043$  Hz we find

$$\tilde{\alpha}^t = -\frac{E_r}{2h} \frac{\Delta\alpha^t}{\alpha} = 0.7 \text{ Hz} \quad (13)$$

**The excitation efficiency and the readout procedure.** After simultaneous excitation of two clock transitions we implement a dedicated readout procedure to deduce the excitation efficiency of each of the transition. Every readout is destructive, i.e. all measured atoms are removed from the trap. Below we use the notation  $|b\rangle$  for the  $|4f^{12}(^3H_5)5d_{3/2}6s^2, J = 9/2\rangle$  level, which is used for the first-stage laser cooling. The relevant thulium levels are shown on Fig. 5a. The sequence of the readout pulses is shown on Fig. 5b.

The readout procedure aims for the measurement of populations of four hyperfine sub-levels  $|g, F = 4\rangle$ ,  $|g, F = 3\rangle$ ,  $|c, F = 3\rangle$  and  $|c, F = 2\rangle$  shown in Fig 5a. The pulse sequence is the following:

1. with the help of 0.2 ms resonant probe 4-5 pulse ( $|g, F = 4\rangle \rightarrow |b, F = 5\rangle$ ) we measure the number of atoms remained in the  $|g, F = 4\rangle$  state after excitation by the "4-3" clock pulse, which is denoted as  $n_{g,4}$ ;
2. by two overlapped 0.7 ms resonant probe 4-5 and 0.5 ms probe 3-4 ( $|g, F = 3\rangle \rightarrow |b, F = 4\rangle$ ) pulses we determine the number of atoms  $n_{g,3}$  remained in the  $|g, F = 3\rangle$  state. The  $|g, F = 3\rangle \rightarrow |b, F = 4\rangle$  pulse repumps atoms from  $|g, F = 3\rangle$  to  $|g, F = 4\rangle$  state;

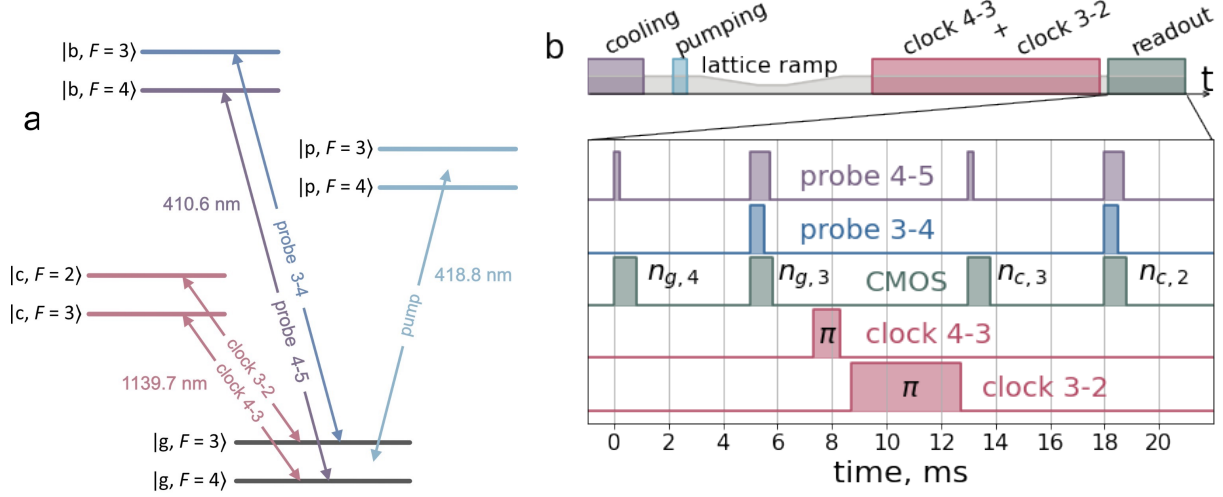


FIG. 5. a) The relevant thulium level scheme. The “pump” radiation is detuned by  $-175$  MHz from  $|g, F = 4\rangle \rightarrow |p, F = 4\rangle$  transition and by  $-90$  MHz from  $|g, F = 3\rangle \rightarrow |p, F = 3\rangle$  transition. b) The measurement cycle (top) and the detailed pulse sequence of the readout procedure (bottom). The “CMOS” line shows the exposition periods of the CMOS camera accumulating the fluorescence signal at  $410$  nm. Labels  $n_{\cdot}$  indicate the signal recorded in the particular camera image. Clock 4-3 and clock 3-2 pulses are the  $\pi$ -pulses which transfer population from the upper clock levels to the ground levels.

3. two consecutive  $\pi$ -pulses clock 4-3 (1 ms duration) and clock 3-2 (4 ms duration) return atoms from  $|c, F = 3\rangle$  to  $|g, F = 4\rangle$  and from  $|c, F = 2\rangle$  to  $|g, F = 3\rangle$  states, respectively;
4. similarly to p.1 we measure  $n_{c,3}$  which is proportional to the number of atoms excited by clock 4-3 pulse;
5. similarly to p.2 we measure  $n_{c,2}$  which is proportional to the number of atoms excited by clock 3-2 pulse.

To accurately determine the excitation efficiencies, we deduce population of the corre-

spending clock levels as following:

$$\begin{aligned}
\tilde{n}_{g,4} &= n_{g,4}, \\
\tilde{n}_{c,3} &= \xi_{c3} \times n_{c,3}, \\
\tilde{n}_{g,3} &= n_{g,3} - \xi_{g3} \times n_{c,3}, \\
\tilde{n}_{c,2} &= \xi_{c2} \times n_{c,2}.
\end{aligned} \tag{14}$$

Here the coefficients  $\xi_{c3}$  and  $\xi_{c2}$  are introduced to account for non-ideal  $\pi$ -pulses and spontaneous decay during the readout time from the clock  $|c\rangle$  to the ground  $|g\rangle$  states. The coefficient  $\xi_{g3}$  takes into account the influence of spontaneous decay from  $|c, F = 3\rangle$  to  $|g, F = 3\rangle$  and  $|g, F = 4\rangle$  during the time interval between the first and the second readout ‘‘CMOS’’ pulses (see Fig. 5b). Note, that population of the  $|c, F = 2\rangle$  level does not affect population of the  $|g, F = 4\rangle$  level, because the transition between them is forbidden. Coefficients  $\xi_{g3}$ ,  $\xi_{c3}$  and  $\xi_{c2}$  are determined from the condition, that the total number of atoms associated with each transition  $\tilde{n}_{g,4} + \tilde{n}_{c,3}$  and  $\tilde{n}_{g,3} + \tilde{n}_{c,2}$  must not depend on the detuning of any of the clock pulses. Using this condition, the coefficients can be determined from the individual scans of the ‘‘4-3’’ and the ‘‘3-2’’ clock transitions shown in Fig. 6a,b.

Finally, the excitation probabilities of each of the clock transitions  $\eta_{43}$  and  $\eta_{32}$  can be calculated as:

$$\eta_{43} = \frac{\tilde{n}_{c,3}}{\tilde{n}_{g,4} + \tilde{n}_{c,3}} = \frac{\xi_{c3} n_{c,3}}{n_{g,4} + \xi_{c3} n_{c,3}}, \tag{15}$$

$$\eta_{32} = \frac{\tilde{n}_{c,2}}{\tilde{n}_{g,3} + \tilde{n}_{c,2}} = \frac{\xi_{c2} n_{c,2}}{n_{g,3} - \xi_{g3} n_{c,3} + \xi_{c2} n_{c,2}}. \tag{16}$$

**Mutual influence of two clock transitions: excitation and readout.** Mutual influence of the clock transitions may occur either (i) from the clock laser fields during the interrogation, or (ii) during the readout procedure.

The first effect (i) is associated with the ac-Stark shift induced by the other interrogation field and equals  $\delta\nu^{\text{AC}} \approx \Omega^2 / (4\pi^2 \Delta\nu_{\text{sep}}) = 0.06 \mu\text{Hz}$  for a 80 ms  $\pi$ -pulse with the Rabi frequency  $\Omega$  and frequency difference  $\Delta\nu_{\text{sep}} = 617 \text{ MHz}$ . Other line pulling effects including quantum interference are also negligible.

The second effect (ii) results from the population transfer between two pairs of clock levels and is much more pronounced for the 3-2 transition. First,  $|g, F = 3, m_F = 0\rangle$  level is initially 10 times less populated than  $|g, F = 4, m_F = 0\rangle$ . Second, the upper level  $|c, F = 3, m_F = 0\rangle$  of the 4-3 transition decays to  $|g, F = 3\rangle$  with 1/28 probability, while the transition from

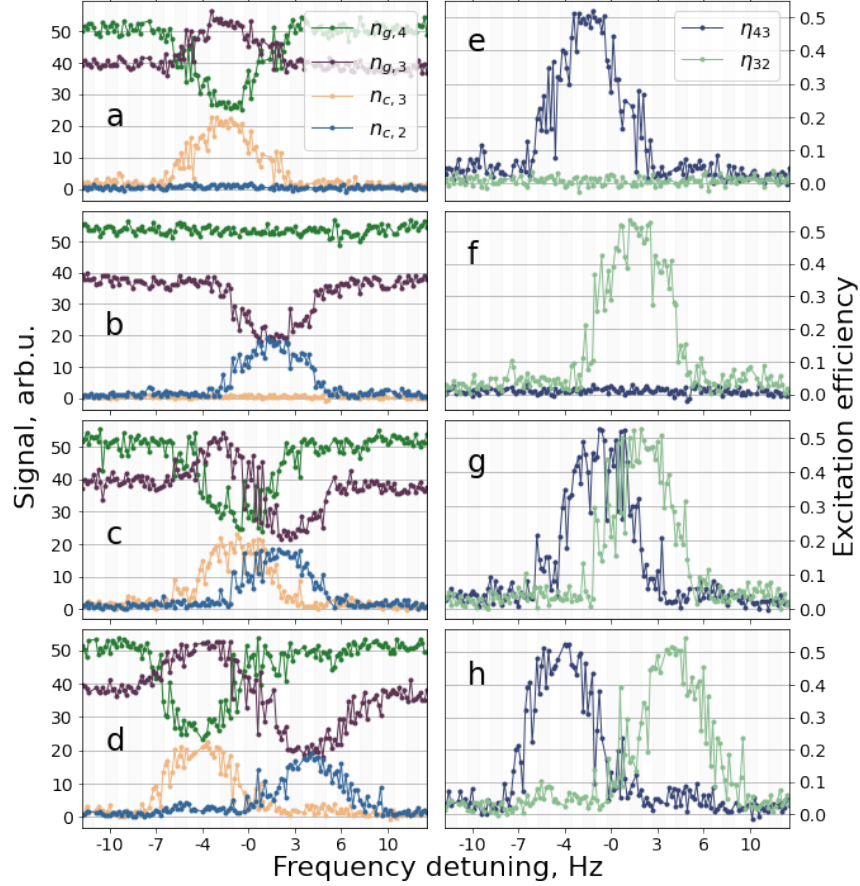


FIG. 6. Simultaneous measurement of excitation probabilities. The left column shows the raw data, the right one shows excitation probabilities deduced from the corresponding raw data using Eqs. 15,16. The first row represents the case when 3-2 excitation field is switched off and only 4-3 transition is excited. The second row shows the case when 3-2 transition is excited solely. In the third and the fourth rows both transitions are scanned using simultaneous excitation procedure. A deliberately introduced additional offset between two interrogating laser fields (3 Hz in the 3rd row and 9 Hz in the 4th row) define the time sequence of passing through two resonance curves. One can see that the resonance profiles are readily recovered both in the case of overlapped resonances and in the case of separate ones.

$|c, F = 2, m_F = 0\rangle$  to  $|g, F = 4\rangle$  is forbidden (Fig. 5a). The effect of population transfer is clearly seen in the raw data in Fig. 6a-d. However, if the timing of excitation and readout procedures remains unchanged, this effect is proportional to the number of atoms excited to the  $|c, F = 3, m_F = 0\rangle$  level and can be eliminated using Eq. 14.

To qualitatively verify this assumption we recorded frequency scans of two resonances

with strong overlapping (c,g) and small overlapping (d,h) as shown in Fig. 6. Generally, the scans of both transitions are independent and are defined by two frequency detunings from the certain  $1.14\ \mu\text{m}$  cavity mode. In this experiment we add a small fixed frequency offset between two interrogation laser fields which defines corresponding scan windows and relative position of resonances in respect to the net frequency difference of 617 MHz. This small offset impacts the relative population of the upper clock levels  $|c, F = 2\rangle$  and  $|c, F = 3\rangle$  right after interrogation procedure. One can see that in both cases the spectral profiles of excitation probability are successfully recovered.

Good agreement of the quadratic Zeeman frequency shift measured at different magnetic field values (Fig. 3) also indicates that the readout procedure correctly recovers spectral profiles of the corresponding clock transitions. The quantitative estimation of the feasible impact of two digital locks is given below.

**The digital lock performance.** Frequency locking of each of the interrogating light fields to the corresponding clock transition is performed by independent tuning of two AOM frequencies as shown in Fig. 1c. For every measurement cycle we simultaneously excite both clock transitions by the bi-colour radiation with each component alternatively detuned by  $+\delta\nu/2$  or  $-\delta\nu/2$  from the central frequency of the corresponding transition. Here  $\delta\nu$  is the measured transition linewidth which in our experiments is equal to 10 Hz. It corresponds to the Fourier spectral width of a 80-ms interrogation pulse. To measure the Zeeman shift at two different magnetic fields  $B_0^r$  and  $B_0^m$  as described in the main text, we change magnetic field after probing excitation efficiencies on the left and right slopes (two consecutive cycles).

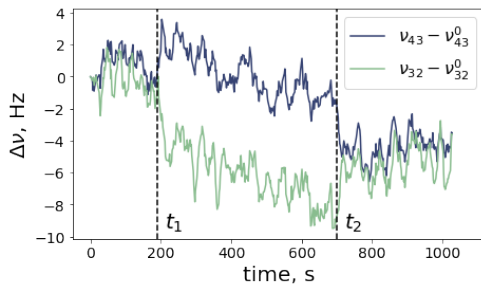


FIG. 7. Response of two parallel frequency lock channels to the instantaneous change of the bias field  $B_0$  from 218 mG to 231 mG at  $t_1 = 190\text{s}$  and back at  $t_2 = 700\text{s}$ .  $\nu_{43}^0$  and  $\nu_{32}^0$  are the corresponding AOMs frequencies at  $t = 0$ . Laser frequency fluctuations and drift are common for both data sets.

Parallel digital lock channels are responsible for two magnetic field values. The integral time constant of the digital proportional-integrating feedback loops equals 100 s.

As a test, we measured response of the digital locks to instantaneous change of the bias magnetic field  $B_0 = 218$  mG by a small value as shown in Fig. 7. At  $t = 190$  s  $B_0$  was increased by  $\Delta B_0 = 13$  mG, and at  $t = 700$  s  $B_0$  was returned to its original value. Two transition frequencies become shifted by the same amount in the opposite directions which corresponds to the estimated Zeeman shift. The typical response time of the digital lock is of 10 s.

To quantitatively evaluate the possible frequency shift from the readout procedure due to the population transfer between the levels we numerically simulated digital locks performance. We generated a set of clock laser frequency signals with random frequency walk and

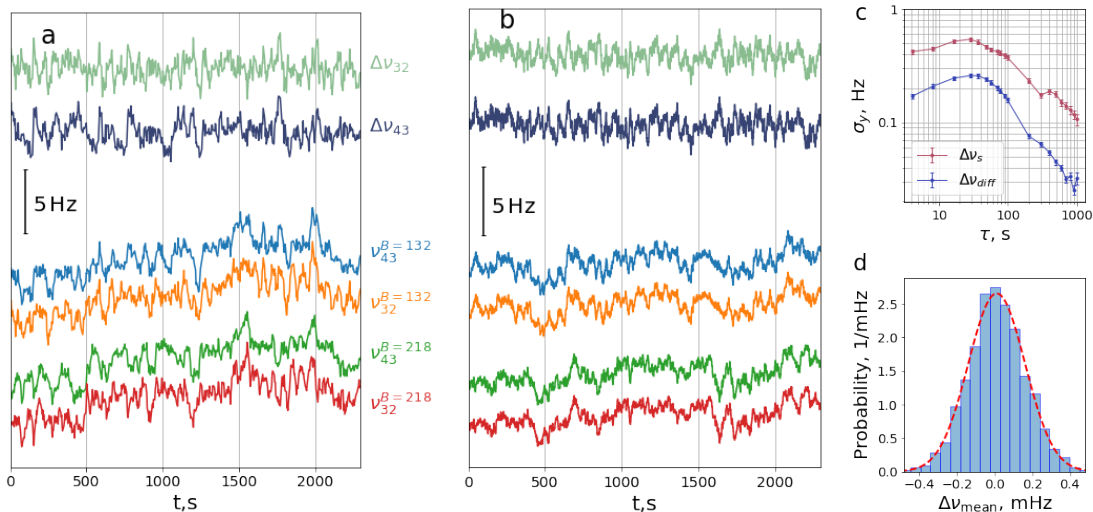


FIG. 8. Experimental frequency traces for  $\Delta\nu_{43}$  and  $\Delta\nu_{32}$  and individual traces  $\nu_{43}(B^m)$ ,  $\nu_{32}(B^m)$ ,  $\nu_{43}(B^f)$  and  $\nu_{32}(B^f)$  for the bias magnetic fields  $B_0^f = 218$  mG and  $B_0^m = 132$  mG (a) and results of simulations (b). Each trace is shifted for visual representation. c) Comparison of the Allan variance plots (experiment) for the synthetic frequency  $\Delta\nu_s = (\Delta\nu_{43} + \Delta\nu_{32})/2$  (red) and the differential frequency  $\Delta\nu_{\text{diff}} = (\Delta\nu_{43} - \Delta\nu_{32})/2$  (blue). d) The histogram of the difference between the 3-2 clock transition line centers from digital frequency locks with the 4-3 interrogation field ON and OFF (simulation). 3000 samples each corresponding for 1 hour data taking is used for the analysis. According to a Gaussian fit, the mean difference equals 12  $\mu\text{Hz}$  with a standard deviation of 150  $\mu\text{Hz}$ .

white phase noise that is similar to the noise pattern of our  $1.14\ \mu\text{m}$  clock laser. The white phase noise broadens the spectral linewidth to about 5 Hz and long-term random frequency walk is usually within 100 Hz during a day. We repeated simulations for different frequency noise levels including those that are considerably higher than in the experiment. Simulation of the digital locks performance in the presence of the laser frequency fluctuations is shown in Fig. 8b together with experimental data (Fig. 8a). Besides the intervals  $\Delta\nu_{43}$  and  $\Delta\nu_{32}$  we show all four transition frequencies at two bias magnetic fields  $B_0^r = 218\ \text{mG}$  and  $B_0^m = 132\ \text{mG}$  for each of the transition. The data comes from four corresponding digital lock channels. Experimental and simulated traces show very similar behaviour. Strong correlation between all four channels indicate that it is the laser frequency fluctuations which are mainly responsible for the short-time instability in Allan plots on figure 2. Comparison of two Allan variance plots for the experimental data on Fig. 8c also demonstrates a 2.8-times higher instability of the synthetic frequency  $\Delta\nu_s = (\Delta\nu_{43} + \Delta\nu_{32})/2$  than of the differential frequency  $\Delta\nu_{\text{diff}} = (\Delta\nu_{43} - \Delta\nu_{32})/2$ . Laser frequency noise should be strongly suppressed in  $\Delta\nu_{\text{diff}}$  which is proven by the data analysis. In turn, magnetic field fluctuations do not significantly contribute to the instability on the given level.

Using this noise model we also compare 3-2 clock transition line centres (deduced from the digital lock operation) for the case of 4-3 excitation radiation switched on and off. The histogram on Fig. 8d consists of 3000 simulation runs each calculated for 1 hour-long data set which is similar to our experimental procedure. In total, the difference between two measurement schemes (4-3 field ON/OFF) equals  $12\ \mu\text{Hz}$  with a standard deviation of  $150\ \mu\text{Hz}$ . This proves that after reasonable averaging time population transfer during the readout does not impact uncertainty of the proposed clock scheme.

**Measurement of the bias magnetic field  $B_0$ .** The magnitude of the bias magnetic field  $B_0$  is deduced from frequency measurements of two transitions  $|g, F = 4, m_F = 0\rangle \rightarrow |c, F = 3, m_F = \pm 1\rangle$  possessing the strong first-order Zeeman sensitivity to the magnetic field. We use the formula

$$B_0 = h \frac{\nu^+ - \nu^-}{2g_F\mu_B}, \quad (17)$$

where  $\nu^+$  and  $\nu^-$  are the frequencies of  $\sigma^+$  ( $|m_F = 0\rangle \rightarrow |m'_F = 1\rangle$ ) and  $\sigma^-$  ( $|m_F = 0\rangle \rightarrow |m'_F = -1\rangle$ ) transitions, respectively,  $g_F = 0.7121$  is Landé g-factor of the  $|c, F = 3\rangle$  level. In the experiment we successively record spectra of the  $\sigma^+$  and  $\sigma^-$  transitions and determine  $\nu^+$  and  $\nu^-$  frequencies (with respect to the frequency of the ULE cavity mode) from the

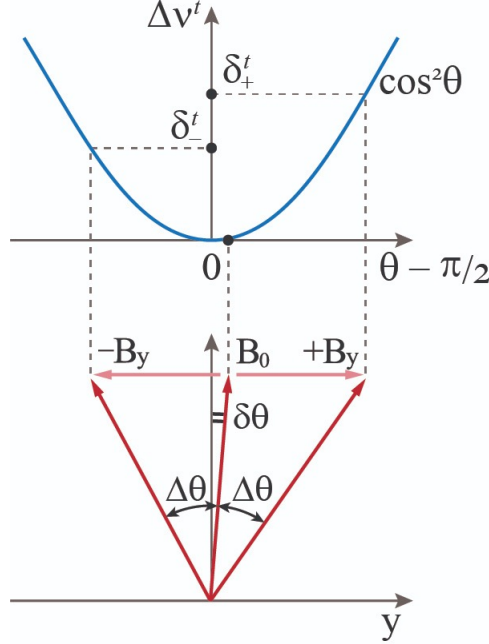


FIG. 9. Sketch of the bias magnetic field direction stabilization. Top: clock 4-3 transition frequency shift as a function of misalignment angle from  $\theta_0 = \pi/2$ . Bottom: orientation of the bias magnetic field for nominal operation (small deviation  $\delta\theta$  from  $\theta_0 = \pi/2$ ) and for calibration measurements  $\pm\Delta\theta$ . Rotation of  $\vec{B}_0$  is accomplished by applying additional  $\pm B_y$  during the clock interrogation period. Misalignment angle  $\delta\theta$  is deduced from the frequency difference  $\delta_{\pm}^t$  according to Eq. 18.

approximations of the corresponding spectra with the Gaussian lineshape. The typical frequency shift  $\nu^+ - \nu^-$  in our experiments was in the range from 140 kHz to 500 kHz. The observed FWHM of  $\sigma^{\pm}$  transitions is about 2 kHz, which can be attributed to the fluctuations of the laboratory magnetic field. Typical statistical uncertainty of the line centre determination from the fit is 200 Hz. From Eq. 17 we estimate the net uncertainty of the magnetic field determination to be  $\sigma_{B_0} = h \frac{\sqrt{2}\delta\nu}{2g_F\mu_B} = 0.14$  mG.

**Stabilization of the magnetic field direction.** To minimize sensitivity of the clock transitions frequencies (both 4-3 and 3-2) to the direction of the bias magnetic field  $B_0$  we chose the angle  $\theta = \pi/2$  (see Fig. 1 and Fig. 9). According to Eq. 4, the sensitivity to angular deviation  $\delta\theta$  at  $\theta = \pi/2$  is quadratic. Variations of the laboratory magnetic field can change the angle  $\theta$ , so one needs to implement an active stabilization. We use a pair of coils producing the field component  $B_y$  which compensates corresponding component of the laboratory field.



To minimize the deviation  $\delta\theta$  we accomplish the following procedure individually for each of the magnetic field values ( $B_0^m$  and  $B_0^r$ ). The procedure is repeated after 5 regular measurement cycles. We intentionally introduce additional angle  $\Delta\theta \approx 0.1$  (the absolute value is not important here) between the field direction and the lattice polarization axis ( $\vec{\epsilon}||y$ ) by changing  $B_y$  at constant value of  $B_x$  (Fig. 9). To change  $B_y$  we add/subtract a fixed current increment  $\Delta I_y$  to the current flowing through the compensation coils. Two transition frequencies  $\nu_+^t$  and  $\nu_-^t$  (for each of the fields  $B_0^m, B_0^r$ ) are measured for  $\theta = \pi/2 + \delta\theta \pm \Delta\theta$  using a standard procedure of interrogating clock 4-3 transition on the left and the right slopes. Frequency shifts  $\delta_{\pm}^t = \nu_{\pm}^t - \nu_{43}$  are calculated with respect to the nominal transition frequency  $\nu_{43}$  at  $\theta = \pi/2 + \delta\theta$  measured in the last measurement cycle. Using Eq. 4,  $\delta\theta$  can be found as

$$\delta\theta = \frac{\delta_+^t - \delta_-^t}{12\tilde{\alpha}^t \Delta\theta (U/E_r)}. \quad (18)$$

For  $\Delta\theta = 0.1$  and  $U = 300 E_r$  the target value of  $|\delta\theta| = 10^{-3}$  is reached for the modest uncertainty of  $|\delta_+^t - \delta_-^t| = 0.4$  Hz, which with our current setup can be achieved in less than 500 cycles of measurement (see Fig. 2b). The single-measurement value  $\delta\theta$  from Eq. 18 is used as an error signal for the proportional-integrational digital lock, which tunes the offset value of  $B_y$  (see Fig. 4a). Thus absolute values of  $\Delta\theta$ , as well as  $\alpha^t$  and  $U/E_r$ , only affect the magnitude of the error signal.